Journal of Power Sources 193 (2009) 924–929

Contents lists available at ScienceDirect

Journal of Power Sources

journal homepage: www.elsevier.com/locate/jpowsour

Preparation and characterization of polypyrrole films for three-dimensional micro supercapacitor

Wei Sun [a,b], Xuyuan Chen [a,b,*]

[a] Institute for Microsystems Technology, Vestfold University College, 3103 Tonsberg, Norway
[b] Pen-Tung Sah MEMS Research Center, Xiamen University, Xiamen 361005, China

ARTICLE INFO

Article history:
Received 31 October 2008
Received in revised form 9 February 2009
Accepted 26 April 2009
Available online 3 May 2009

Keywords:
Supercapacitor
Polypyrrole
Three-dimensional
Geometric capacitance

ABSTRACT

As electro-active electrodes for supercapacitors, micro polypyrrole (PPy) films doping with ClO_4^- (PPy_{ClO_4}) and Cl^- (PPy_{Cl}) are prepared on Ni layers modified three-dimensional (3D) structures in Si substrates. The key process to fabricate the 3D structures is high-aspect-ratio deep reactive ion etching, which result in significant increase of available surface area. Homogeneous conformal Ni layers and PPy films are deposited on the 3D structures by electroless plating and electropolymerization, respectively. The supercapacitor properties of PPy films are investigated by using cyclic voltammetry (CV), electrochemical impedance spectroscopy (EIS) and galvanostatic charge/discharge with three-electrode system in NaCl solution. It is shown that doping with ClO_4^- results in ideal supercapacitor behaviors with rectangle-like CV shapes at scan rates from 5 to 200 mV s^{-1}, linear galvanostatic charge/discharge curves at current loads from 0.5 to 2 mA and stable cyclic property. However, doping with Cl^- gives rise to non-ideal properties of supercapacitor. SEM of the PPy_{ClO_4} shows that the surface of the PPy_{ClO_4} electrode is smooth and the thickness of the PPy_{ClO_4} film is about 2.5 μm. The geometric capacitance of PPy_{ClO_4} is calculated as 0.030 F cm^{-2} from CV at scan rate of 100 mV s^{-1}, 0.023 F cm^{-2} from EIS and 0.027 F cm^{-2} from galvanostatic discharge at 1 mA cm^{-2} current density.

1. Introduction

Miniaturized devices using microelectromechanical system (MEMS) technologies have led to requests for miniaturized power sources. Great efforts have been made to develop microbatteries [1–3] and energy harvesters [4,5]. For instance, Nathan's group fabricated a three-dimensional (3D) thin film microbattery for autonomous MEMS [3], which has much higher capacity than planar thin film battery. However, such a 3D thin film microbattery still cannot shadow MEMS supercapacitor in application where high power is required.

As an energy storage device with high power density, MEMS supercapacitor can be used not only to replace microbattery, but also to be coupled to microbattery or energy harvester to provide peak power. Double layer supercapacitors composed of interconnected silver particles and with a high frequency response (200 Hz) were fabricated by Brevnov and Olson [6], which had geometric capacitance (capacitance per unit the electrode geometric area) of 1.7 mF cm^{-2}. However, the value of the capacitance is not big enough for long time discharging because the double layer supercapacitor is established by electrostatic attraction at the interface of electrolyte and electrode. With the working principle different from the double layer supercapacitors, the electrochemical supercapacitors have larger capacitance which produced by rapidly doping/undoping of ions into thin layers of electro-active material. The electro-active material could be electrically conducting polymers, such as polyaniline, polypyrrole, polythiophene and their derivatives [7–10]. Among them, polypyrrole (PPy) is considered one of the most promising electrode materials of supercapacitors due to the advantages of facile synthesis, low cost, environmentally friendliness and high capacitance [7]. As a key parameter, the capacitance of PPy electrode can be affected by the type, size and valence of the ions in preparing and testing solutions [11]. PPy doping with ClO_4^- presented more ideal supercapacitor properties than that of NO^{3-} was reported by Song et al. [12]. PPy doping with polysulfonated aromatic anions had the geometric capacitance of 0.40 F cm^{-2} was presented by Ingram [13], with the thickness of 10 μm. The geometric capacitance properties of PPy electrode can be also improved by increasing the electrode area. So far, research groups worldwide have mainly focused on optimization of PPy preparing conditions and composites based on PPy, such as PPy/carbon nanotube, to modify the morphology of the electrode [14,15]. But there is

* Corresponding author at: Vestfold University College, Institute for Microsystems Technology, Raveien 197, Horten, 3103 Vestfold, Norway. Tel.: +47 3303 1161; fax: +47 3303 1103.
E-mail address: xuyuan.chen@hive.no (X. Chen).

0378-7753/$ – see front matter © 2009 Elsevier B.V. All rights reserved.
doi:10.1016/j.jpowsour.2009.04.063

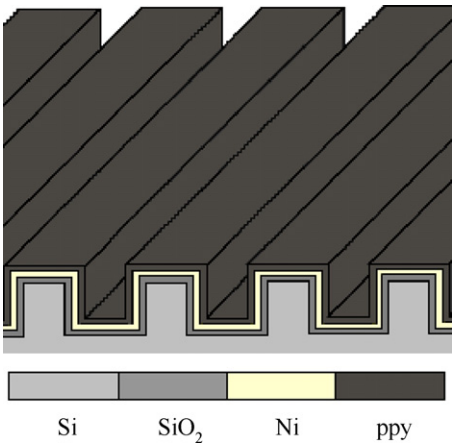

Fig. 1. Schematic drawing of the 3D electrode.

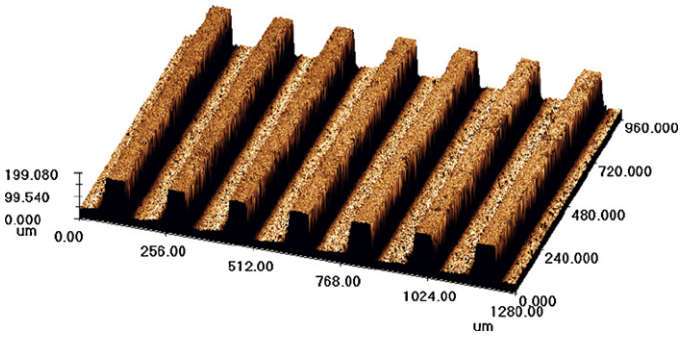

Fig. 2. Image of nickel films on 3D structure.

much less attention on increasing the capacitance of supercapacitor through structuring the supercapacitor with big effective surface area per unit volume of the supercapacitor.

In this study, a 3D structure was designed for achieving the big effective surface area and fabricated by using DRIE technology. Conformal Ni layers and PPy films were deposited on the 3D structure to form current collectors and electro-active material. The PPy electrodes doping with different anions were investigated by electrochemical methods to characterize their supercapacitor properties.

2. Design and experimental

2.1. Design of 3D electrodes

The electrodes of MEMS supercapacitors with 3D structures were designed as shown in Fig. 1, which is fabricated in a Si substrate. Conformal Ni current collectors and electro-active PPy films were deposited on the 3D structures to form the 3D electrodes for the supercapacitor. The 3D structure has periodic channels which result in significant increase of effective surface area for the 3D electrodes. For a square Si wafer, according to the 3D design, the surface area gain (AG) can be calculated by Eq. (1):

$$AG = \frac{S_{3D}}{S_{planar}} = L\left(\frac{2H + W_c + W_w}{W_c + W_w}\right)\frac{L}{L^2} = 1 + \frac{2H}{W_c + W_w} \quad (1)$$

where S_{3D}, S_{planar}, L, H, W_c and W_w are the surface area of the 3D electrode, the surface area of the similarly planar electrode, the side length of the wafer, the depth of each channel, the width of each channel, and the each inter-channel space, respectively. It is apparently that the AG depends on the aspect ratio, so the high-aspect-ratio deep reactive ion etching (DRIE) is used to etch the substrates. In this study, L, H, W_c and W_w equals 1 cm, 150, 120 and 60 μm, respectively. Thus we can achieve $AG = 2.7$.

For depositing the conformal Ni current collectors, electroless plating process has been developed. Traditional metal deposition techniques such as RF sputtering cannot be used because they are not conformal processes. For growing the conformal PPy electro-active material films, electrochemical polymerization was carried out in solutions with different anions. The detail fabrication processes are described in the following text.

2.2. Fabrication of the 3D structure in Si substrate

At first, a Al layer with 400 nm thickness was deposited on cleaned Si substrate by RF sputtering. Secondly, the Al layer was structured with finger-like pattern by photolithography and wet etching, to be used as DRIE protection mask. Thirdly, the high-aspect-ratio process DRIE was carried out by AMS200 (Alcatel, France) to form the 3D structure, by using SF_6 as etching gas and C_4F_8 as passivation gas, we achieved a 3.95 μm per minute etching speed with aspect ratio of 1.25. Finally, conformal 1.5 μm thick SiO_2 layer formed as the insulator by thermal oxidation.

2.3. Electroless plating of Ni layers

We have build up electroless plating setup and successfully develop the process for conformal Ni film deposition on SiO_2 layer on the 3D structure. Before Ni electroless plating, the pre-treatment steps including coarsening, sensitization, activation which were carried out to increase the roughness of SiO_2 surface, to absorb the reductive Sn^{2+} ions, and to form the Pd initial nuclear, respectively. The electroless plating was performed in a bath working at 90–100 °C which containing 240 g l^{-1} $NiSO_4$, 160 g l^{-1} sodium succinate, 110 g l^{-1} NaCl, 50 g l^{-1} $MgSO_4$, 50 g l^{-1} NaH_2PO_2 and 30 g l^{-1} malic acid. After 30 min, the continuous and homogeneous Ni film was obtained on the 3D structure, as shown in Fig. 2.

2.4. Polymerization of PPy films

PPy films doping with Cl^- and ClO_4^- anions (PPy_{Cl} and PPy_{ClO_4}) were galvanostatically prepared on the Ni current collectors in solution containing 0.1 M pyrrole (Py) monomer and 0.5 M supporting salts of NaCl and $LiClO_4$, respectively. Platinum sheets were used as cathode. Py (Fluka, 99%) was purified by vacuum distillation prior to use, all other reagents were obtained from commercial sources and were used as received. The pH of each electrolytic cell was adjusted at 4.00 by the corresponding acid and alkaline. The polymerizations were carried out at 20 °C and 1 mA current for 30 min. From the SEM view in Fig. 3, we can see that the surface of the PPy_{ClO_4} is smooth and the thickness of the PPy_{ClO_4} is about 2.5 μm.

2.5. Characterization of PPy electrodes

Cyclic voltammetry (CV), electrochemical impedance spectroscopy (EIS) and galvanostatic charge/discharge were used to investigate the supercapacitor properties of PPy_{Cl} and PPy_{ClO_4}. All the electrochemical tests were performed on electrochemical workstation (Solartron 1260) in a three-electrode system with the Pt sheet as counter electrode and saturated calomel electrode (SCE) as reference electrode in 1 M KCl solution, all the potentials which will be mentioned later are versus SEC.

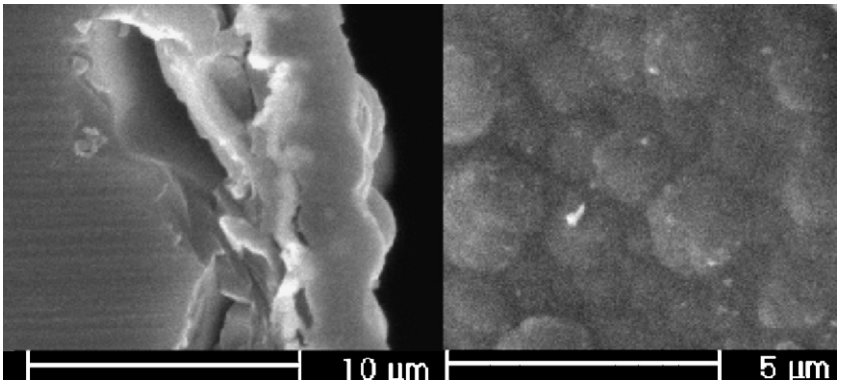

Fig. 3. SEM view of PPy_{ClO_4}.

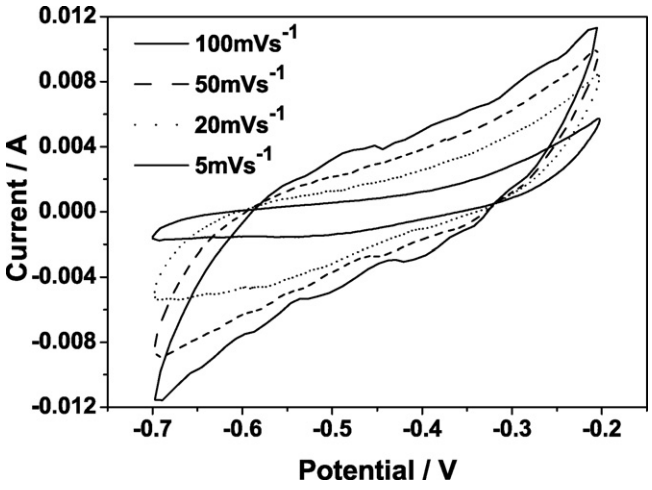

Fig. 4. CV curves of PPy_{Cl} electrode.

3. Results and discussions

3.1. CV tests

The CV tests were carried from −1.0 to −0.5 V for PPy_{ClO_4} and from −0.7 to −0.2 V for PPy_{Cl} with the scan rates of 5, 20, 50, 100, 200 and 500 mV s^{-1}. The potential ranges were determined by the linear part of galvanostatic charge/discharge curves. Figs. 4 and 5 present the CV curves of PPy_{Cl} and PPy_{ClO_4}, respectively. All the curves were obtained between 5th and 20th cycle to make sure that the PPy films were activated but not degenerated. We found that the maximum Faradic current of PPy_{Cl} is larger than that of PPy_{ClO_4} at the same scan rate, but the shape of CV curves for PPy_{Cl} is non-ideal. However, the shape of CV curves for PPy_{ClO_4} is rectangle-like, which is the characteristic of electrochemical capacitors. The size of Cl^- is smaller than ClO_4^-, so Cl^- in testing solution can easily replace ClO_4^- to insert into and eject from the PPy matrix during cycling. Therefore PPy_{ClO_4} present batter supercapacitor properties in NaCl testing solution. For a supercapacitor with rectangle-like CV shape (current is almost a constant), the quantitative geometric capacitance C of the electrode can be calculated approximately by Eq. (2):

$$C = \frac{Q}{UA} = \frac{It}{UA} = \frac{I}{UA/t} = \frac{I}{SA} \quad (2)$$

where the Q is the total charges in PPy electrode, U is the potential window of the CV test, A is the geometric surface of substrate, I is the absolute value of the anodic or cathodic current in CV curves, t is the time of half charging or discharging cycle, and S is the voltage scan rate. Fig. 6 presents the geometric capacitances of PPy_{ClO_4} at scan rates of 5, 20, 50, 100, 200 and 500 mV s^{-1}. It is shown that the geometric capacitance drop rapidly (from 0.064 to 0.030 F cm^{-2}) with scan rate increasing from 5 to 100 mV s^{-1}, but slowly with scan rate increasing from 100 to 500 mV s^{-1} (0.014 F cm^{-2}). At slow scan rate, ion doping/undoping is finished completely over long time, resulting in large capacitance. While at fast scan rate, the charge diffusion cannot follow the change of electric field, which gives rise to smaller geometric capacitance.

More than 800 cycles CV test was carried out to characterize the cyclic behavior of PPy_{ClO_4}. The reactive current as a function of cycle number is given in Fig. 7. It is observed that the reactive current did not decrease apparently even the cycle number up to

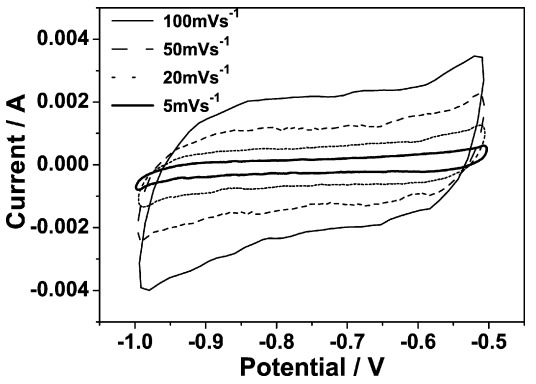

Fig. 5. CV curves of PPy_{ClO_4} electrode.

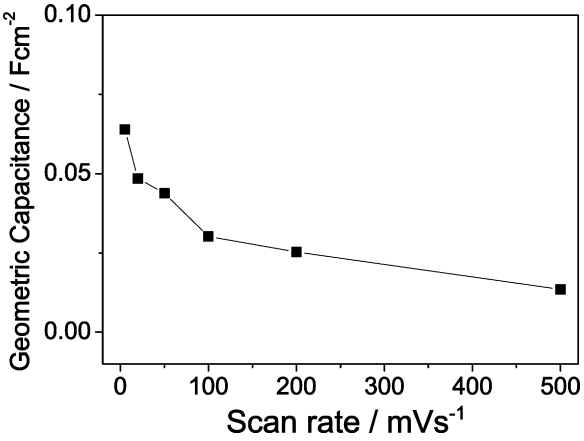

Fig. 6. Geometric capacitance of PPy_{ClO_4} at various scan rates.

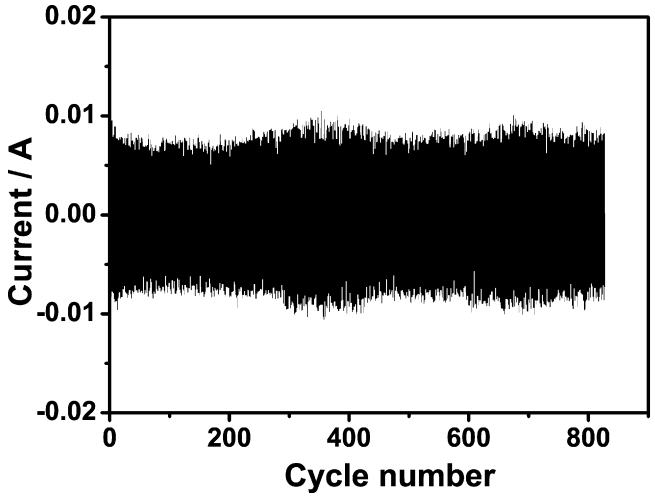

Fig. 7. Reactive current versus cycle number.

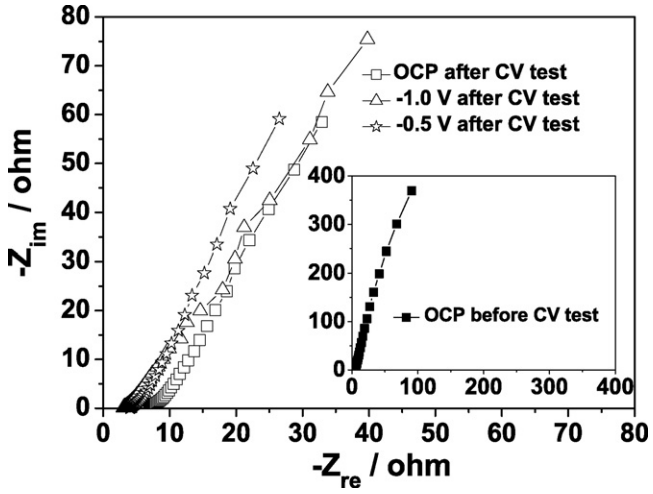

Fig. 9. Nyquist plots of the PPy_{ClO_4} electrode at different potentials.

more than 800, which means almost no geometric capacitance lose. At the about 300th cycle, there is a little increase of reactive current. This is because during long time soaking, PPy matrix absorbed more solution, and thus the ions diffusion distance became shorter. CV curves at scan rate of 50 mV s^{-1} before and after long time cycling are presented in Fig. 8. It is found that the two CV curves are almost overlapping, which implied that there is almost no geometric capacitance degenerated after 800 cycles. Therefore, the PPy_{ClO_4} we prepared has very stable cyclic behavior.

3.2. EIS test

The PPy_{ClO_4} electrode was also investigated by EIS test over a frequency range from 100 mHz to 100 kHz and with potential amplitude of 10 mV. Before any CV tests, the Nyquist plot of PPy_{ClO_4} at open circuit potential (OCP) is shown as insert in Fig. 9, a decline line were observed at low frequency area. The angles between the decline lines and the real axes are large than 45° and lower than 90°, corresponding the ion diffusion mechanism between Warburg diffusion and ideal capacitive ion diffusion. Fig. 9 also presents the Nyquist plots of PPy_{ClO_4} electrode at OCP, −1.0 V (undoping state) and −0.5 V (doping state) after 800 times cycling. We found the three decline lines are close to each others at low frequencies implying both doping and undoping states of PPy_{ClO_4} electrode have the similar geometric capacitance.

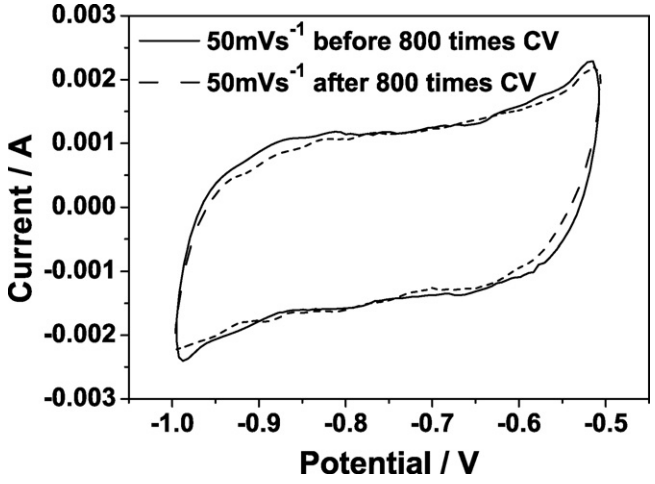

Fig. 8. CV curves of PPy_{ClO_4} before and after 800 cycles at scan rate of 50 mV s^{-1}.

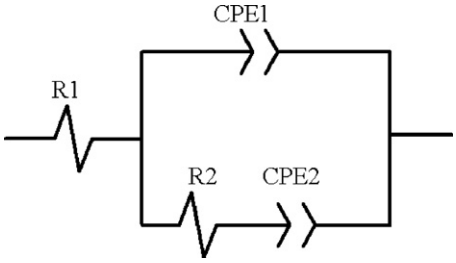

Fig. 10. Equivalent circuit for modeling.

The EIS data can be fitted by the equivalent circuit shown in Fig. 10, in which R_1 means the resistance of solution and wires, R_2 characterizes the charge transfer resistance between the interface of the test solution and PPy_{ClO_4} film, CPE_1 and CPE_2 instead of capacitors to describe the double layer capacitance at the interface, and the pseudo capacitance from ions transfer in the PPy matrix. Figs. 11 and 12 present the modeling curves of the Nyquist plots obtained before and after long time cycling at OCP. From the modeling results, the geometric capacitance of the PPy_{ClO_4} is 0.004 F cm^{-2} before long time cycling, which is far less than 0.0023 F cm^{-2}, the value that is obtained after 800 times CV cycling. This is because before long time cycling, the ClO_4^- ions were the active ions, however, the Cl^- ions replace the ClO_4^- to dope and undope during long time cycling.

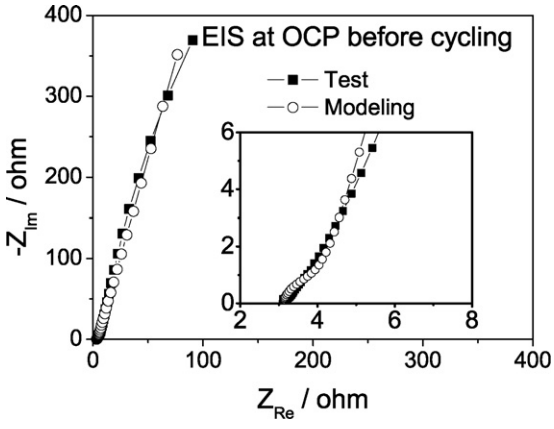

Fig. 11. Modeling result of PPy_{ClO_4} electrode before 800 times cycling at OCP.

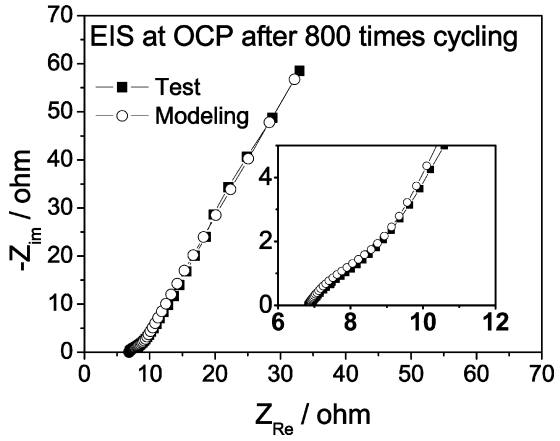

Fig. 12. Modeling result of PPy_{ClO_4} electrode after 800 times cycling at OCP.

The geometric output power of the electrode P can be obtained from Eq. (3):

$$P = \frac{0.5CU^2 - I^2Rt}{t} \quad (3)$$

where U is the potential window of the CV test, C the geometric capacitance, I is the absolute value of the anodic or cathodic current in CV curves, t is the time of half charging or discharging cycle, and R is the sum of R_1 and R_2. Therefore, the geometric output power depends on R. From the modeling results, R equal 8.8 and 11.8 ohm before and after 800 times cycling, the value that make the second item in numerator is far less than the first one on the right side of Eq. (3). With the CV scan rate of 100 mV s^{-1}, the geometric output power is 0.708 mW.

3.3. Galvanostatic charge/discharge test

Galvanostatic charge/discharge technique was also used to characterize the supercapacitor performance for PPy_{Cl} and PPy_{ClO_4} electrodes. The data were obtained from −1.0 to −0.5 V for PPy_{ClO_4} electrode and from −0.7 to −0.2 V for PPy_{Cl} electrode, at the charge/discharge current densities of 2, 1 and 0.5 mA cm^{-2}. The charge/discharge curves of PPy_{ClO_4} electrode is shown in Fig. 13, we found the curves are almost linear in the whole potential range at various current rates, which indicates that the PPy_{ClO_4} electrode has a good supercapacitor properties. The discharge geometric capacitance C can be calculated from the linear part of discharge curve by

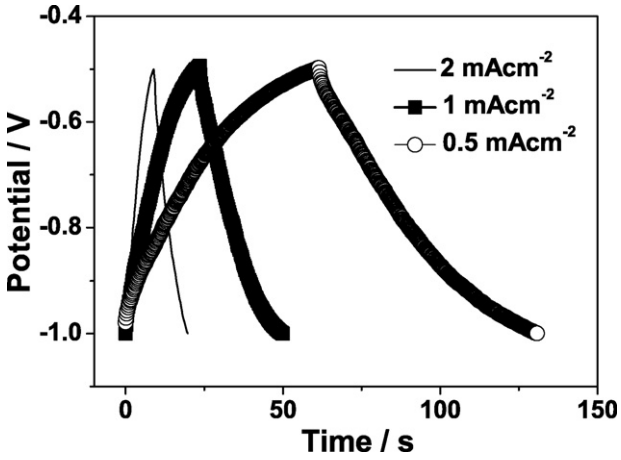

Fig. 13. Galvanostatic charge/discharge curve of PPy_{ClO_4}.

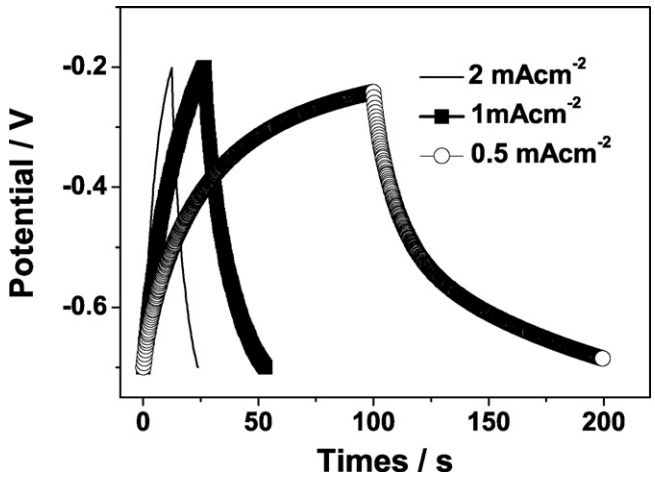

Fig. 14. Galvanostatic charge/discharge curve of PPy_{Cl}.

Eq. (4):

$$C = \frac{It}{UA} \quad (4)$$

where I is the discharge current density, t is the discharge time, U is the potential window of discharging and A is the geometric surface of substrate. The PPy_{ClO_4} electrode presented 0.011, 0.027 and 0.070 F cm^{-2} geometric capacitances at 2, 1 and 0.5 mA cm^{-2} discharge current densities, respectively.

Fig. 14 presents galvanostatic charge/discharge curves of PPy_{Cl}. The nearly linear lines were observed at 2 and 1 mA cm^{-2} current densities, but much more bending curve was obtained while current density of 0.5 mA cm^{-2} was applied (the potential window was shortened as −0.7 to −0.25 V). The PPy_{Cl} electrode presented the behavior of non-ideal supercapacitor at current of 0.5 mA.

4. Conclusions

The electrodes for MEMS supercapacitor were designed with a 3D structure which consists of conformal Ni current collectors and PPy electro-active films. The 3D structure was fabricated by high-aspect-ratio DRIE process. We achieved big effective surface area with surface area gain of 2.7. Electroless plating process has been successfully developed for conformal deposition of Ni current collectors. Electropolymerization method has been used to form PPy electro-active films doping with ClO_4^- (PPy_{ClO_4}) and Cl^- (PPy_{Cl}) in $LiClO_4$ and NaCl solutions. Both PPy_{ClO_4} and PPy_{Cl} electrodes were investigated by using electrochemical methods in NaCl solution. Doping with ClO_4^- results in ideal supercapacitor behaviors, e.g. rectangle-like CV shapes at scan rates from 5 to 200 mV s^{-1}, linear galvanostatic charge/discharge curves at current loads from 0.5 to 2 mA and stable cyclic property. However, doping with Cl^- gives rise to non-ideal properties of supercapacitor. The geometric capacitance of PPy_{ClO_4} electrode is calculated as 0.030 F cm^{-2} from CV test at scan rate of 100 mV s^{-1}, 0.023 F cm^{-2} from EIS and 0.027 F cm^{-2} from galvanostatic discharge at 1 mA cm^{-2} current density, with the PPy_{ClO_4} thickness of about 2.5 μm. The 3D PPy_{ClO_4} is a promising material for making electrode of MEMS supercapacitor.

Acknowledgements

The research was funded by Institute for Microsystems Technology at Vestfold University College. The MEMS fabrication was supported by Pen-Tung Sah MEMS research center in Xiamen University. The electrochemical tests were supported by State Key

laboratory for Physical chemistry of solid surfaces in Xiamen University.

References

[1] M.S. Park, G.X. Wang, H.K. Liu, S.X. Dou, Electrochimica Acta 51 (2006) 5246–5249.
[2] C.L. Liao, K.Z. Fung, Journal of Power Sources 128 (2004) 263–269.
[3] M. Nathan, D. Golodnitsky, V. Yufit, E. Strauss, T. Ripenbein, I. Shechtman, S. Menkin, E. Peled, Journal of Microelectromechanical Systems 14 (2005) 879–885.
[4] M. Marzencki, A. Yasser, B. Skandar, Sensors and Actuators A 145–146 (2008) 363–370.
[5] M. Ferrari, V. Ferrari, M. Guizzetti, D. Marioli, A. Taroni, Sensors and Actuators A 142 (2008) 329–335.
[6] D.A. Brevnov, T.S. Olson, Electrochimica Acta 51 (2006) 1172–1177.
[7] Y.L. Xu, J. Wang, W. Sun, S.H. Wang, Journal of Power Sources 159 (2006) 370–373.
[8] K. Rajendra Prasad, N. Munichandraiah, Journal of Power Sources 112 (2002) 443–451.
[9] J.H. Sung, S.J. Kim, K.H. Lee, Journal of Power Sources 126 (2004) 258–267.
[10] A. Laforgue, P. Simon, C. Sarrazin, J.F. Fauvarque, Journal of Power Sources 80 (1999) 142–148.
[11] C. Weidlich, K.M. Mangold, K. Juttner, Electrochimica Acta 50 (2005) 1547–1552.
[12] S.H. Song, D.S. Han, H.J. Lee, H.S. Cho, S.M. Chang, J.M. Kim, H. Muramatsu, Synthetic Metals 117 (2001) 137–139.
[13] M.D. Ingram, H. Staesche, K.S. Ryder, Journal of Power Sources 129 (2004) 107–112.
[14] J.Y. Kim, K.H. Kim, K.B. Kim, Journal of Power Sources 176 (2008) 396–402.
[15] J. Wang, Y.L. Xu, X. Chen, X.F. Sun, Composites Science and Technology 67 (2007) 2981–2985.